Sedimentology (2006) **53,** 1265–1287 doi: 10.1111/j.1365-3091.2006.00812.x

Channel formation by flow stripping: large-scale scour features along the Monterey East Channel and their relation to sediment waves

ANDREA FILDANI*[1], WILLIAM R. NORMARK†, SVETLANA KOSTIC‡[2] and GARY PARKER‡[2]
**Department of Geological and Environmental Sciences, Stanford University, Stanford, CA 94305, USA (andf@chevrontexaco.com)*
†U. S. Geological Survey, Menlo Park, CA 94025, USA
‡St Anthony Falls Laboratory, University of Minnesota, Minneapolis, MN 55414, USA

ABSTRACT

The Monterey East system is formed by large-scale sediment waves deposited as a result of flows stripped from the deeply incised Monterey fan valley (Monterey Channel) at the apex of the Shepard Meander. The system is dissected by a linear series of steps that take the form of scour-shaped depressions ranging from 3·5 to 4·5 km in width, 3 to 6 km in length and from 80 to 200 m in depth. These giant scours are aligned downstream from a breech in the levee on the southern side of the Shepard Meander. The floor of the breech is only 150 m above the floor of the Monterey fan valley but more than 100 m below the levee crests resulting in significant flow stripping. Numerical modeling suggests that the steps in the Monterey East system were created by Froude-supercritical turbidity currents stripped from the main flow in the Monterey channel itself. Froude-supercritical flow over an erodible bed can be subject to an instability that gives rise to the formation of cyclic steps, i.e. trains of upstream-migrating steps bounded upstream and downstream by hydraulic jumps in the flow above them. The flow that creates these steps may be net-erosional or net-depositional. In the former case it gives rise to trains of scours such as those in the Monterey East system, and in the latter case it gives rise to the familiar trains of upstream-migrating sediment waves commonly seen on submarine levees. The Monterey East system provides a unique opportunity to introduce the concept of cyclic steps in the submarine environment to study processes that might result in channel initiation on modern submarine fans.

Keywords Cyclic steps, deep-water channel formation, flow stripping, megascours, numerical modeling, sediment waves, turbidity currents.

INTRODUCTION

Early work on the Monterey Fan was focused on the prominent fan channel extending from Monterey Canyon (Dill *et al.*, 1954; Menard, 1955; Shepard, 1966). However, the modern Monterey Fan has been fed by two major canyon systems, Monterey and Ascension (channels A and M, Fig. 1). Much of the prominent depositional relief (levee/overbank) of the upper fan was related to the Ascension Canyon system (Normark, 1970a). More recent work on the channel systems of the upper fan focused on overbank deposits and their bedforms and on channel processes (Hess &

[1]Present address: Chevron ETC, San Ramon, CA 94583, USA.
[2]Present address: Ven Te Chow Hydrosystems Laboratory, University of Illinois, Urbana-Champaign, IL 61801, USA.

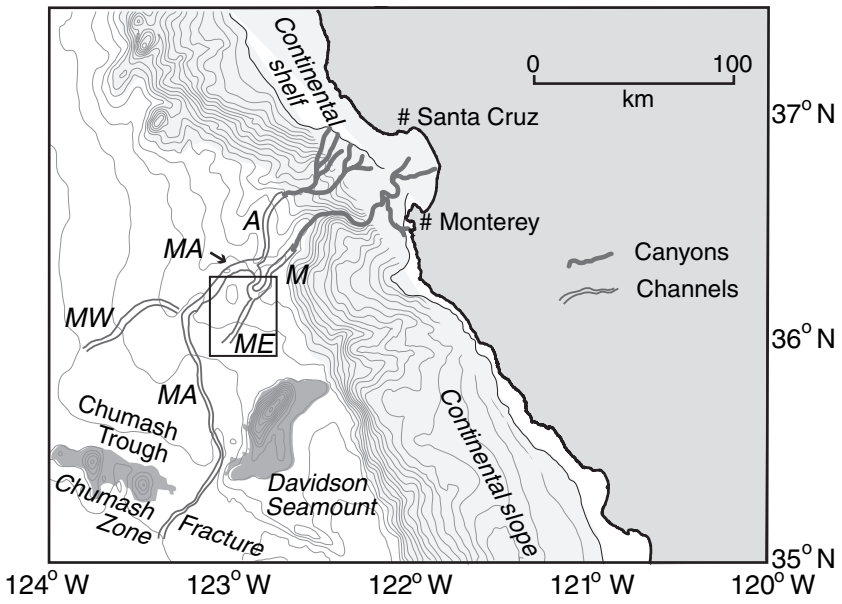

Fig. 1. Schematic map of Monterey Fan and its major channels on the upper fan: A, Ascension; M, Monterey, ME, Monterey East; MA, Monterey Ascension; MW, Monterey West (terminology from Fildani & Normark, 2004). Bold rectangle shows Fig. 2.

Normark, 1976; McHugh *et al.*, 1992; McHugh & Ryan, 2000). The Monterey channel is contiguous with the lower part of the Ascension fan valley, however, erosion of as much as 250 m has significantly deepened the Ascension valley downstream of their confluence (identified as MA in Fig. 1; Normark, 1999).

Using seismic-reflection profiling, Fildani & Normark (2004) provided a stratigraphic framework for the Monterey Fan in which two main turbiditic systems were recognized: a Lower Turbidite System, which was fed by canyons north of the Ascension and Monterey systems, and the much younger Upper Turbidite System (UTS). The morphology of the UTS and the development of the multiple channels in effect constitute the deposit identified as the modern Monterey Fan in earlier studies (e.g. Normark *et al.*, 1985).

The improved understanding of channel history on the Monterey Fan has been supported by the development of new mapping and imaging techniques ranging from deep-tow geophysical surveys of small areas to fan-wide long-range sidescan imagery and multibeam bathymetry. These new data integrated with seismic-reflection profiles show that the Monterey East depositional system is composed of large-scale bedforms that are dissected by a channel-like feature (incipient channel of Fildani & Normark, 2004). Modern mapping techniques show that the Monterey East channel, as interpreted originally, does not have a continuous thalweg but instead is formed by a series of deep, discontinuous scours. Fig. 2 shows the detailed bathymetry and location of seismic-reflection tracklines in the area of the Monterey East channel feature, and Fig. 3 shows the bathymetric profile along the axis of the line of large flute-shaped depressions.

The focus of this paper is to understand the processes that form the large scours and perhaps lead to the formation of a channel. Because no continuous channel feature exists (or existed in the past), the term Monterey East system is used to include the area on the outside of the Shepard Meander (Shepard, 1966) that is characterized by large-scale sediment waves and the giant scours (Fig. 2).

The data available for this study include: seismic-reflection profiles (single-channel and 3·5 kHz), multibeam bathymetric data, deep-tow side-scan images, and stratigraphic control provided by sediment core samples. Data details and characteristics are described in Fildani & Normark (2004).

MONTEREY EAST SYSTEM

Multibeam bathymetry shows that the Monterey East giant scours extend as much as 30 km and form the centerline of a 30 km-wide area characterized by large-scale bedforms that are interpreted herein as sediment waves that are generally concentric around the Shepard Meander (McHugh & Ryan, 2000; Fildani & Normark, 2004). The sediment-wave field, which is dissected by the aligned train of giant scours, lies

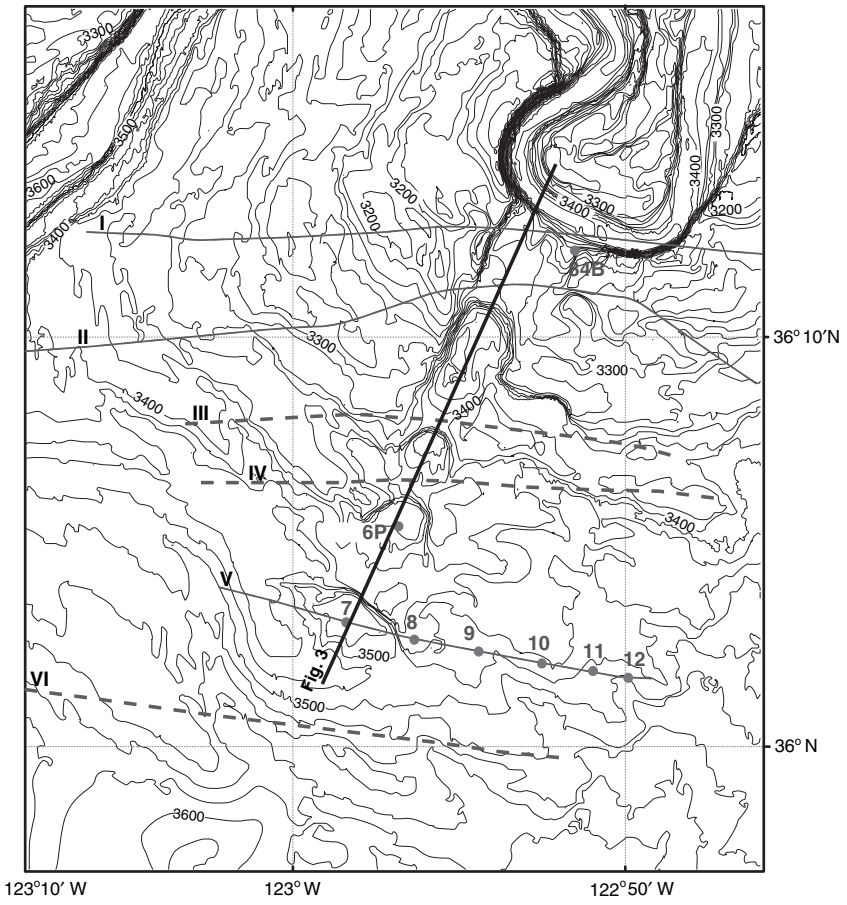

Fig. 2. Multibeam bathymetric map (in metres) showing Monterey East flute-shaped scours and sediment cores. Location of seafloor profile of Fig. 3 is shown. Tracklines for seismic-reflection profiles available for this study are shown as dashed lines and illustrated profiles in Fig. 4 are solid lines. Core locations for sediment logs in Fig. 7 are shown for free-fall (boomerang) cores (7 through 11) and piston core 6P.

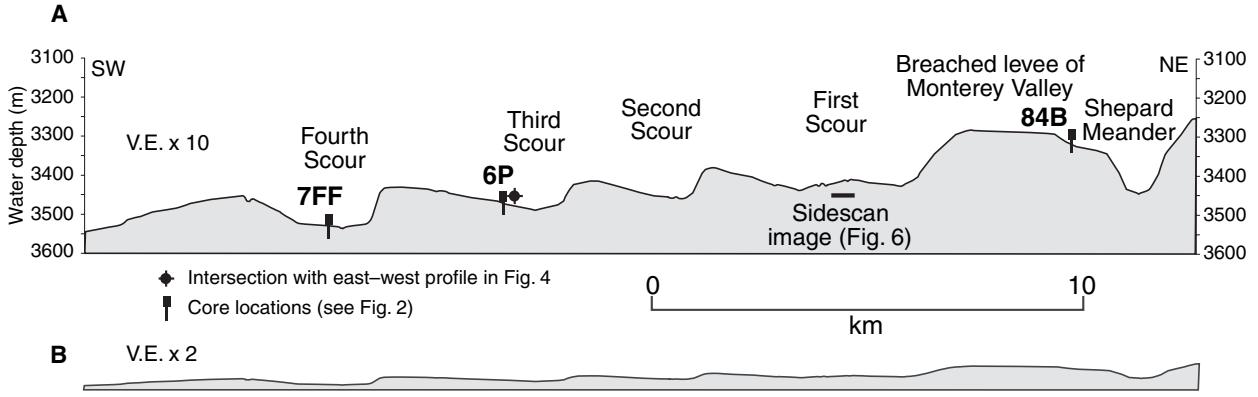

Fig. 3. Axial bathymetric profile constructed from the multibeam bathymetric data shown in Fig. 2 showing core locations for those along profile. See Fig. 2 for location.

more than 200 m above the floor of the modern erosional Monterey channel (Fig. 2). The chute through the levee crest at the head of the line of scours is at least 160 m lower than the adjacent levee crest (Fig. 2 and line I in Fig. 4A). The location of the chute could be related to an early failure of the Monterey levee crest. To the west, the sediment-wave field is bordered by the deeply eroded modern MA fan valley (upper corner of Fig. 2); to the east and south, the ME-related deposits are buried by the Sur submarine slide of probable Holocene age (Normark & Gutmacher, 1988).

The Monterey East scours shallow and broaden down fan (Figs 2 and 5); they vary in size and shape, ranging from 3·5 to 4·5 km in width, 3 to

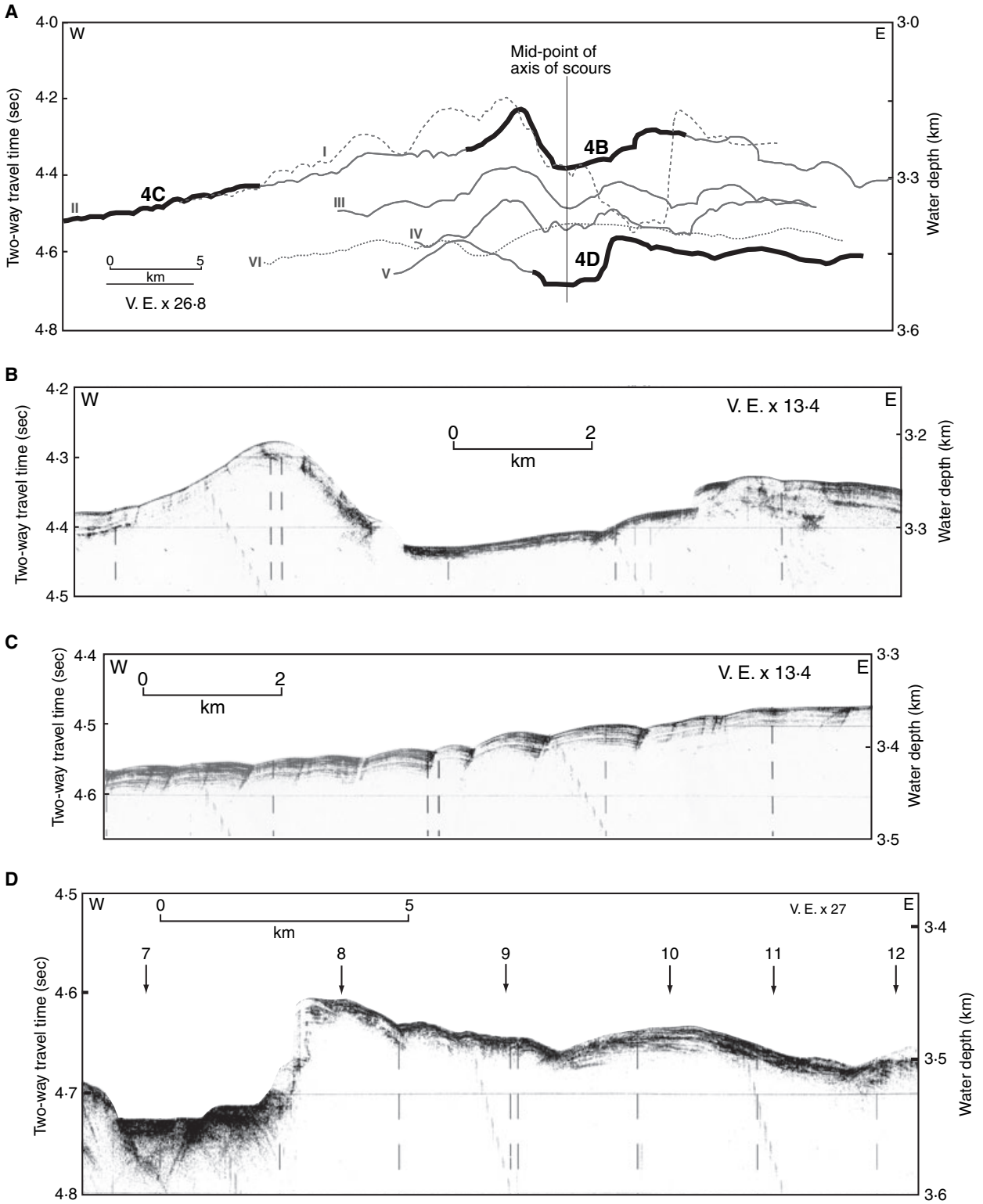

Fig. 4. East-west 3·5 kHz high-resolution profiles. (A) Line drawings of seafloor profile from 3·5 kHz records showing the highly variable morphology of the Monterey East system. Bold line shows profiles illustrated in 4 B, C and D. See Fig. 2 for location.

6 km in length, and they are as much as 200 m deep (Figs 2 and 3). A longitudinal profile along the axis of the channel-like feature shows the cyclic step-like character of these scours (Fig. 3B). High scarps that form the upslope and lateral margins contrast with gentle, lower-relief slopes

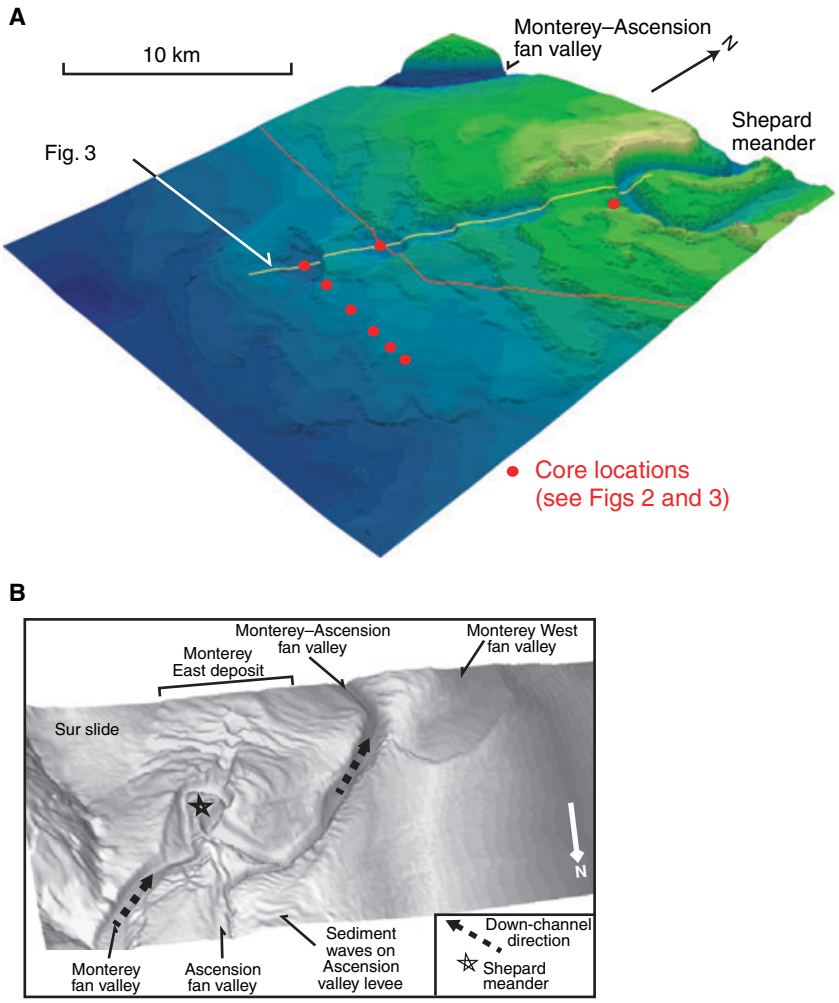

Fig. 5. (A) Shaded relief image (constructed from multibeam bathymetric data) of the area in Fig. 2 with core locations shown; solid red-line is Fig. 4A in Fildani & Normark (2004). This image emphasizes the discontinuous channel floor character of Monterey East. (B) Shaded relief image (view from north) of the upper Monterey Fan showing the channel systems identified in Fig. 1. The high vertical exaggeration is to enhance the large-scale sediment waves and scours. Adapted from Fildani & Normark (2004).

along their southern (down-slope) margins resulting in distinctive flute-shaped depressions in plan view.

High-resolution seismic-reflection profiles that were obtained to better define a channel feature instead intersected the Monterey East giant scours orthogonally and showed poorly developed or non-existent levee-like relief (Fig. 4A and B). Fig. 4A illustrates the highly variable nature of the seafloor expression of the scour lineament in a series of crossings plotted on the same depth (vertical) axis. There is no continuous gradient along the 'channel' trend and adjacent sounding lines show marked changes in width, depth, and reflection character (compare crossings in Fig. 4B and D; see location of tracklines in Fig. 2).

The well-developed sediment waves form an arcuate pattern about the curvature of the Shepard Meander and flank the line of scours. Seismic-reflection profiles show evidence of upslope migration by asymmetric sediment deposition across the wave crests (Fig. 4C and their morphology is best seen in the high vertical exaggeration of the south-looking shaded-relief image in Fig. 5B). Deep-tow side-looking sonar images, 3·5 kHz reflection profiles supplemented by multibeam bathymetry, and sediment core samples indicate that the area containing and surrounding the scours has experienced recent activity, including erosive action, sand deposition, and/or sediment reworking represented by dune fields as imaged by deep-tow sonars (Fig. 6). Fig. 6B shows a sonograph from deep-tow sonar of sediment waves imaged inside one of the large scours. These bedforms are probably formed by diluted flows (i.e. tails of major flows).

Core samples from both Scripps Institution of Oceanography and the USGS are short (<10 m) compared with the depth of the scours, but they show evidence of recent turbidity currents preserved on the Monterey East area (Fig. 7). Turbidite deposition of sand and silt is common, even

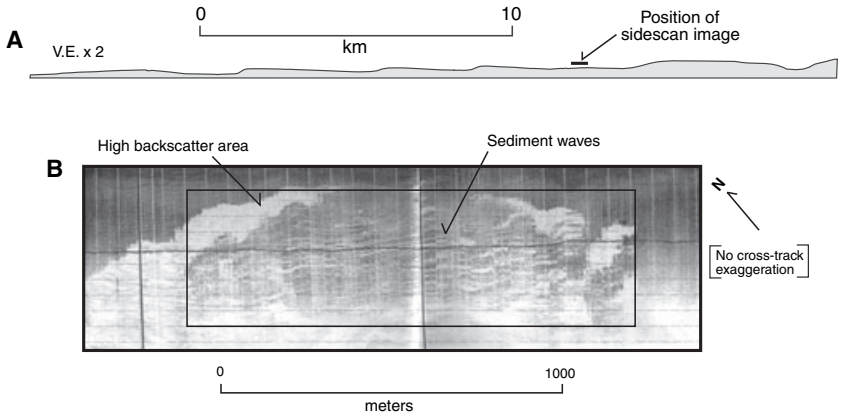

Fig. 6. Deep-tow sidescan (100 kHz) sonograph of smaller scale sediment waves located in the scour closest to the Shepard Meander. This image was obtained with sidescan 50 m above the seafloor. High backscatter area is interpreted as the scarps of the large scour. More details can be found in Hess & Normark (1976).

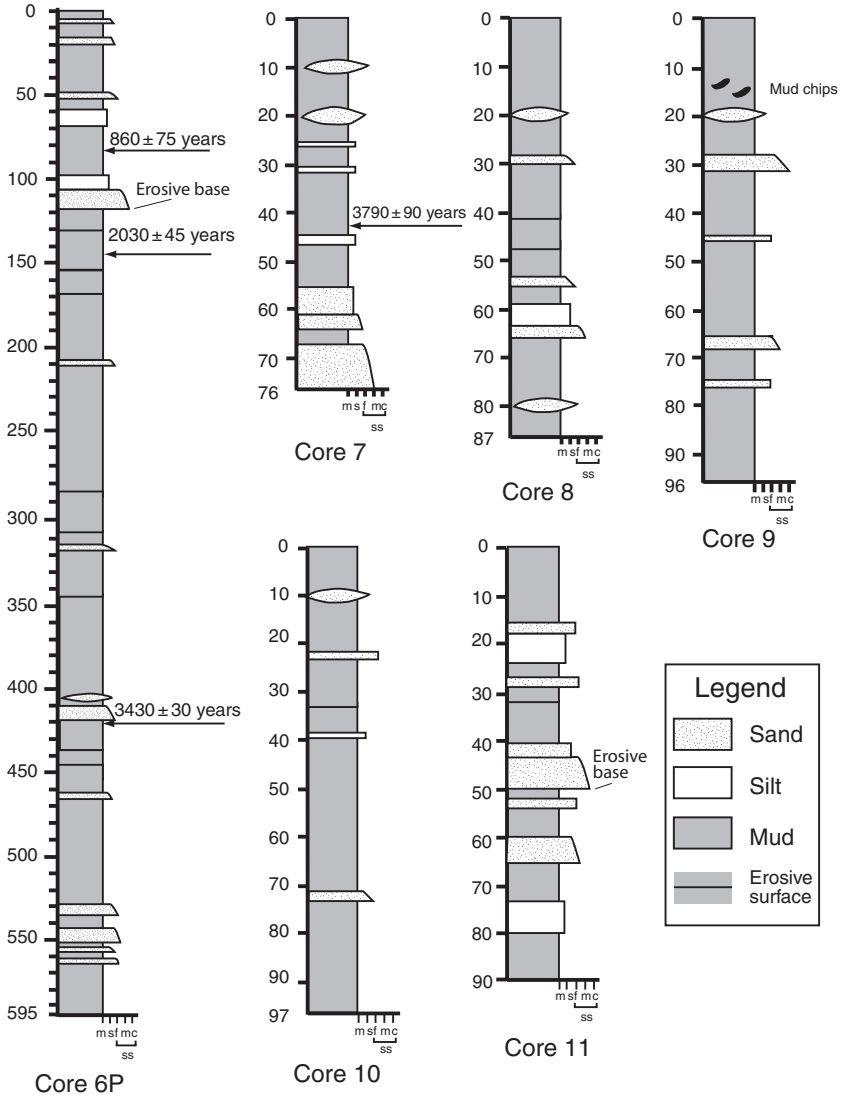

Fig. 7. Sedimentary logs for piston and free-fall cores from Monterey East feature showing available radiocarbon dates. Core locations in Figs 2, 3 and 5. m, mud; s, silt; ss, sandstone (f = fine, m = medium, c = coarse).

in the short free-fall cores (Fig. 7). Single turbiditic events deposited normally-graded medium-sand to fine-sand beds with sharp or erosive bases (Fig. 7). Sand beds up to ~10 cm were recognized in both piston and free-fall (boomerang) cores. Laminations and traction structures (faint ripples)

are present. Some silt/mud turbidites have also been documented because of their characteristic sharp base and normal grading into mud. Bioturbation in the hemipelagic intervals is present but not common. These fine-grained turbidites represent the upper part of the turbidity currents flowing through the Monterey fan valley that have been flow-stripped (*sensu* Piper & Normark, 1983) at the chute leading from the Shepard Meander to the chain of scours. Radiocarbon dating of foraminifera from interbedded hemipelagic mud in two of the cores shows that flow stripping is common throughout the Holocene. Preliminary results show late Holocene accumulation rates of as much as 1·2 m ka^{-1}. In contrast, the sediment accumulation rate on the high western levee of the MA channel immediately downstream from the Shepard Meander is only about 25% of the rate for Monterey East (see Discussion in Normark, 1999). Radiocarbon dating confirms that the Monterey East system is probably the most active depositional area on the upper fan.

The linear chain of giant scours on the Monterey East system are unlike scour fields found on the modern San Lucas or Navy fans (Normark, 1970b; Normark *et al.*, 1979) or in Ross Formation of the Upper Carboniferous (Elliott, 2002; Lien *et al.*, 2003). Although the scour dimensions are comparable for the three modern fans, only the Monterey East scours form locked in a linear train. On the San Lucas and Navy fans, scour fields are found over a broad area in the channel-lobe transition zone (*sensu* Mutti & Normark, 1987); they formed as flows went through a break in slope and underwent lateral spreading upon leaving the fan channel. The scours of the Ross Formation are one to two orders of magnitude smaller than those of the Monterey East and they do not form a linear sequence of steps, although they are thought to form from flow stripping (Lien *et al.*, 2003).

MONTEREY EAST SCOURS: ANALOG TO FLUVIAL CYCLIC STEPS

The Monterey East scours take the form of a train of four steps incised into a levee/overbank area associated with the outer bend of the Shepard Meander of the Monterey Channel (Figs 3 and 5). Much of this area is covered with a field of large-scale sediment waves (Fildani & Normark, 2004). The geomorphic features displayed in Fig. 5 can be reasonably assumed to be the results of the passage of successive turbidity currents, e. g., turbidity currents from the Monterey channel built its levee, the sediment wave field, and the scour holes. The steps of the ME scours describe a pattern of downdip undulation that is similar to the sediment waves of the adjacent levee. They differ in three ways; (i) the steps of the ME scours have a longer characteristic wavelength, or spacing, than the sediment waves ($3 \sim 6$ km vs. $1 \sim 3{\cdot}5$ km); (ii) they appear to be incisional rather than depositional features; and (c) the holes of the steps are bounded on the updip side by scarps that are noticeably steeper than the corresponding points on the sediment waves. However, these differences may be superficial features that mask a fundamental similarity in terms of the morphodynamics that created them.

The steps of the Monterey East system are not unique if it is considered that they may have analogs in the sub-aerial setting as well as in the results of open channel flume and tank experiments. Discontinuous gullies cut into cohesive material provide an excellent example of incisional cyclic steps (Reid, 1989). Bedrock streams often display similar trains of incisional steps (Fig. 8A; Wohl, 2000). Incisional cyclic steps have been explained theoretically (Parker & Izumi, 2000) and modelled in the laboratory (Fig. 8B, Koyama & Ikeda, 1998; Brooks, 2001). Cyclic steps are schematized in Fig. 9 showing that each step is defined at its upstream and downstream end by a hydraulic jump, or a short zone over which the flow makes a rapid conversion from shallow, swift supercritical flow ($\mathbf{Fr} > 1$) to deep, tranquil sub-critical flow ($\mathbf{Fr} < 1$). Cyclic steps in alluvium have also been observed in the field (Winterwerp *et al.*, 1992) and in the laboratory (Fig. 8C, Taki & Parker, 2005), and explained theoretically by Sun and Parker (2005) using a formulation that parallels the incisional analysis of Parker & Izumi (2000). Cyclic steps in alluvium can form under conditions of bed aggradation or degradation, or they may simply migrate updip in the absence of net bed level change.

Of particular relevance here are antidunes. Antidune trains are trains of bed waves for which the bed undulations are approximately in phase with the undulations of the water surface; that is, the water surface is high where the bed is high, and the water surface is low where the bed is low (Fig. 9A). To a first approximation, antidunes can be characterized as rhythmic bedforms that are (i) associated with Froude-supercritical flow; and (ii) migrate upstream. For rivers the Froude number **Fr** is a dimensionless number defined as:

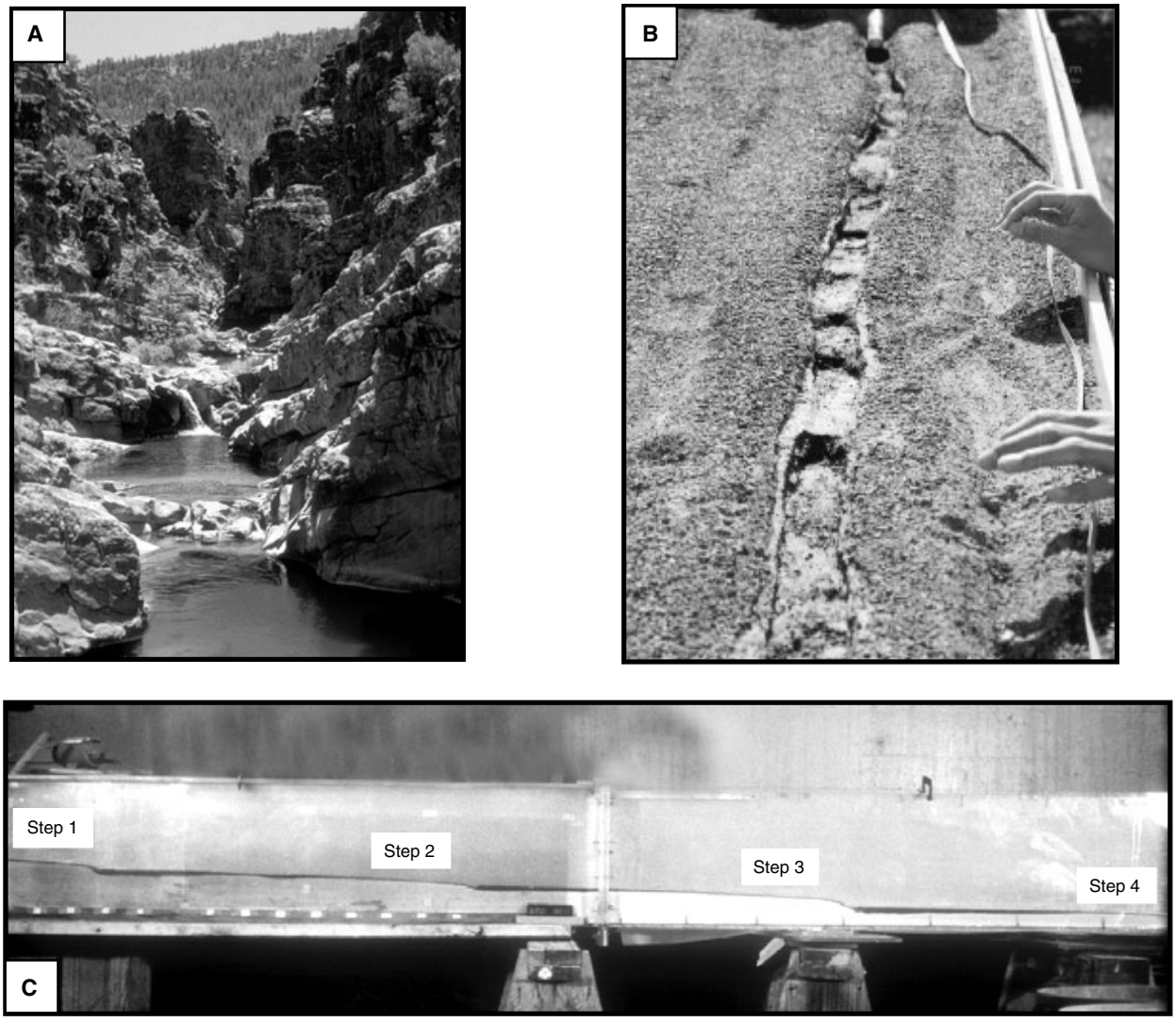

Fig. 8. (A) Cyclic steps in a bedrock channel, Big Box Canyon, Arizona, USA (Wohl, 2000). Image courtesy E. Wohl. (B) Experimental cyclic steps in a model bedrock (Koyama & Ikeda, 1998). Image courtesy H. Ikeda. (C) Alluvial cyclic steps in the laboratory; channel length is 4 m. From Taki and Parker (2005).

$$\mathbf{Fr} = \frac{U}{\sqrt{gh}} \qquad (1)$$

where h denotes flow depth, U denotes depth-averaged flow velocity and g denotes the gravitational acceleration. A river flow is supercritical if $\mathbf{Fr} > 1$. This corresponds to a very swift flow.

However, the description of antidunes stated above is not completely accurate because antidunes can occur in flows with Froude numbers that are less than unity using the definition in Eq. (1). This is because most fluvial antidunes have relatively short wavelengths, which allow the effective local Froude number to drop somewhat below the long-wave (shallow-water) value described by Eq. (1) (e.g. Engelund & Fredsoe, 1982). In addition, there are conditions under which antidunes can migrate downstream, (e.g. Engelund, 1970). Nevertheless, the characterization given in the previous paragraph is sufficient for the purposes of comparison between sub-aerial and submarine conditions.

Submarine sediment waves have been characterized variously as antidunes or antidune-like features associated with turbidity currents (e.g. Lee *et al.*, 2002; Normark *et al.*, 2002), largely because seismic-reflection profiles show updip migration. However, the flows that created them have not been directly observed. The waves differ strongly in at least one way from the standard picture of fluvial antidunes. Fluvial antidunes tend to be ephemeral features that initiate, form

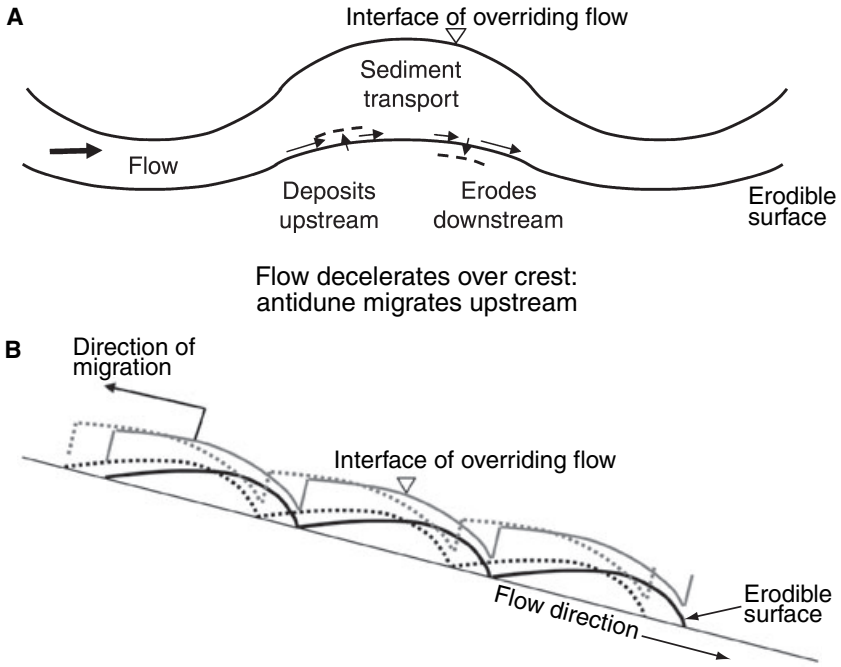

Fig. 9. (A) Diagram illustrating upstream-migrating antidunes, with deeper, slower flow over the crests and shallower, swifter flow over the troughs. (B) Diagram illustrating upstream-migrating fluvial cyclic steps, for which the flow over each step is bounded both upstream and downstream by a hydraulic jump.

into trains, grow in amplitude, and then suddenly break and are obliterated. The cycle is then repeated at a different location. As a result, fluvial antidunes rarely leave a depositional record that shows a clear and coherent train of waveforms migrating upstream. Rather, fluvial antidune stratification is characterized by faint, poorly-defined laminae (e.g. Prothero & Schwab, 1996). Fluvial antidunes generally do not leave the coherent train of updip-migrating features such as those on Monterey Fan.

However, recently, a rhythmic fluvial bedform has been identified which (i) migrates upstream as a coherent, quasi-permanent train; and (ii) is a close relative of the antidune. These bedforms have been termed 'cyclic steps' by Parker & Izumi (2000). In Fig. 9B each step is defined at its upstream and downstream end by a hydraulic jump, or a short zone over which the flow makes a rapid conversion from shallow, swift supercritical flow ($\mathbf{Fr} > 1$) to deep, tranquil sub-critical flow ($\mathbf{Fr} < 1$). Each step may be divided into two parts bounded by a point where $\mathbf{Fr} = 1$; an upstream sub-critical zone and a downstream supercritical zone. The slower sub-critical zone induces net sediment deposition (or enhanced deposition or suppressed incision), and the faster supercritical zone includes net sediment erosion (or suppressed deposition or enhanced incision), so that the entire train migrates upstream (Parker & Izumi, 2000).

Cyclic steps are relatives of antidunes, and as such are a manifestation of the fact that supercritical flow over an erodible bed is inherently unstable. Two features distinguish them from classical fluvial antidunes; (a) cyclic steps are long-wave phenomena, so that the wavelength is one or two orders of magnitude larger than the flow depth, so that the local critical Froude number is indeed given accurately by Eq. (1), and (b) the presence of the hydraulic jumps stabilizes the wave train, so that it can march upstream as a self-preserving train. As a result, cyclic steps, as opposed to classical antidunes, have the potential to leave a coherent depositional record as a train of waveforms.

APPLICATION TO THE MONTEREY EAST SYSTEM

From rivers to turbidity currents

Froude-supercritical flows are relatively rare in alluvial river channels. In the sub-aerial setting, they become common only in steep, bedrock channels. However, submarine turbidity currents are intrinsically more biased toward supercritical flow than rivers. The densimetric Froude number $\mathbf{Fr}_d$ for a turbidity current can be defined as:

$$\mathbf{Fr}_d = \frac{U}{\sqrt{RCgh}} \qquad (2)$$

where h is now an appropriate measure of turbidity current thickness, C is the layer-averaged volume

concentration of suspended sediment carried by the turbidity current and R is the submerged specific gravity of the sediment, given as:

$$R = \frac{\rho_s}{\rho} - 1 \quad (3)$$

where ρ_s is sediment density and ρ is water density. For most natural sediments R is close to 1·65. More precise definitions for layer thickness h and layer-averaged flow velocity U and volume suspended sediment concentration C are given below.

Turbidity currents, as opposed to submarine debrisflows, are dilute suspensions, so that $C << 1$, and thus $RC << 1$. Comparing Eqs (2) and (1), it is seen that for the same values of flow velocity U and current thickness (depth) h, a turbidity current is biased toward a higher (densimetric) Froude number than a river. This does not mean that sub-critical turbidity currents cannot form; both sub-critical and supercritical turbidity currents are observed in the laboratory (e.g. Garcia, 1993) and both have been inferred in the field (e.g. Pirmez & Imran, 2003). On the other hand, it does mean that supercritical turbidity currents should be common, especially at higher seafloor slopes.

The numerous sediment wave fields of Monterey, including those adjacent to the ME scours, are now considered (Fig. 5B; see Normark *et al.*, 2002; Fildani & Normark, 2004). These fields are formed on levees where a turbidity current is presumed to have overflowed from a channel. Slopes down the levee (away from the channel axis) tend to be considerably steeper than slopes down the channel. A steeper slope generates a swifter flow that is more likely to be Froude-supercritical. The result is a setting that is prone for the formation of cyclic steps. This flow would give rise to upstream-migrating cyclic steps corresponding to sediment waves. The antidune interpretation is more precisely elaborated with the cyclic-step concept. Cyclic steps can be accurately characterized as long-wave antidunes that are locked in sequence by the hydraulic jumps. It is this locking that can allow for orderly updip migration, and thus preservation of the train in the stratigraphic record.

Now a change in flow regime is considered in a way that a flow-stripped turbidity current becomes competent to establish net-erosional conditions. Such a change might be caused by an increase in the thickness of the turbidity currents carried by the main channel. A low spot in the levee field (created by a crevasse or by slumping) would focus a net-erosional flow possibly excavating a proto-channel. As long as the flow is still Froude-supercritical, this net erosion can be expected to be accompanied by upstream-migrating cyclic steps. The wavelength of the steps should be different from the net-depositional steps (sediment waves) on the adjacent levee because the formative flow would be different. In addition, as the turbidity current erodes into the levee surface it should encounter sediment layers with increasing resistance to erosion as a result of consolidation. In the sub-aerial setting, steps incising into material with intrinsic strength such as clay or bedrock develop distinct steps or depressions bounded on the upstream side by well-defined scarps. These same scarps are apparent in Fig. 10, which is based on Fig. 3 but in which an interpretation of the overriding flow has been added.

Parameterization of turbidity currents

The case of interest is turbidity currents on a levee that are formed by stripping of the upper part of a channelized flow. The configuration is specified in Fig. 11A. The overflowing turbidity current is approximated as a sheet moving down the levee perpendicular to the channel flow from which it is stripped. Flow stripping occurs on the outside of a channel bend, where flow momentum causes the unchannelized upper part of the flow to continue in a direction close to that upchannel from the bend.

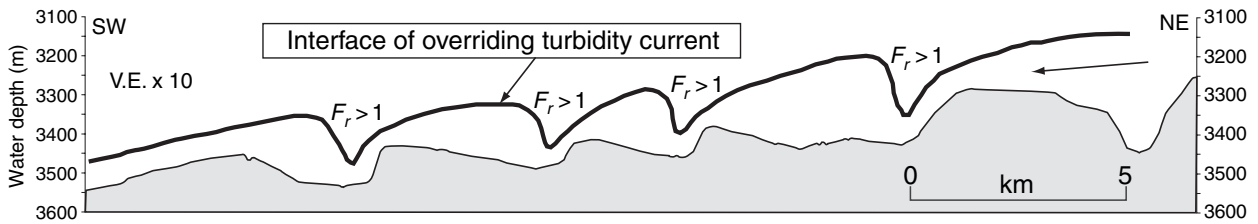

Fig. 10. Conceptual illustration of the upper interface of the net-erosional turbidity current that may have created the train of scours of the Monterey East system (based on Fig. 3).

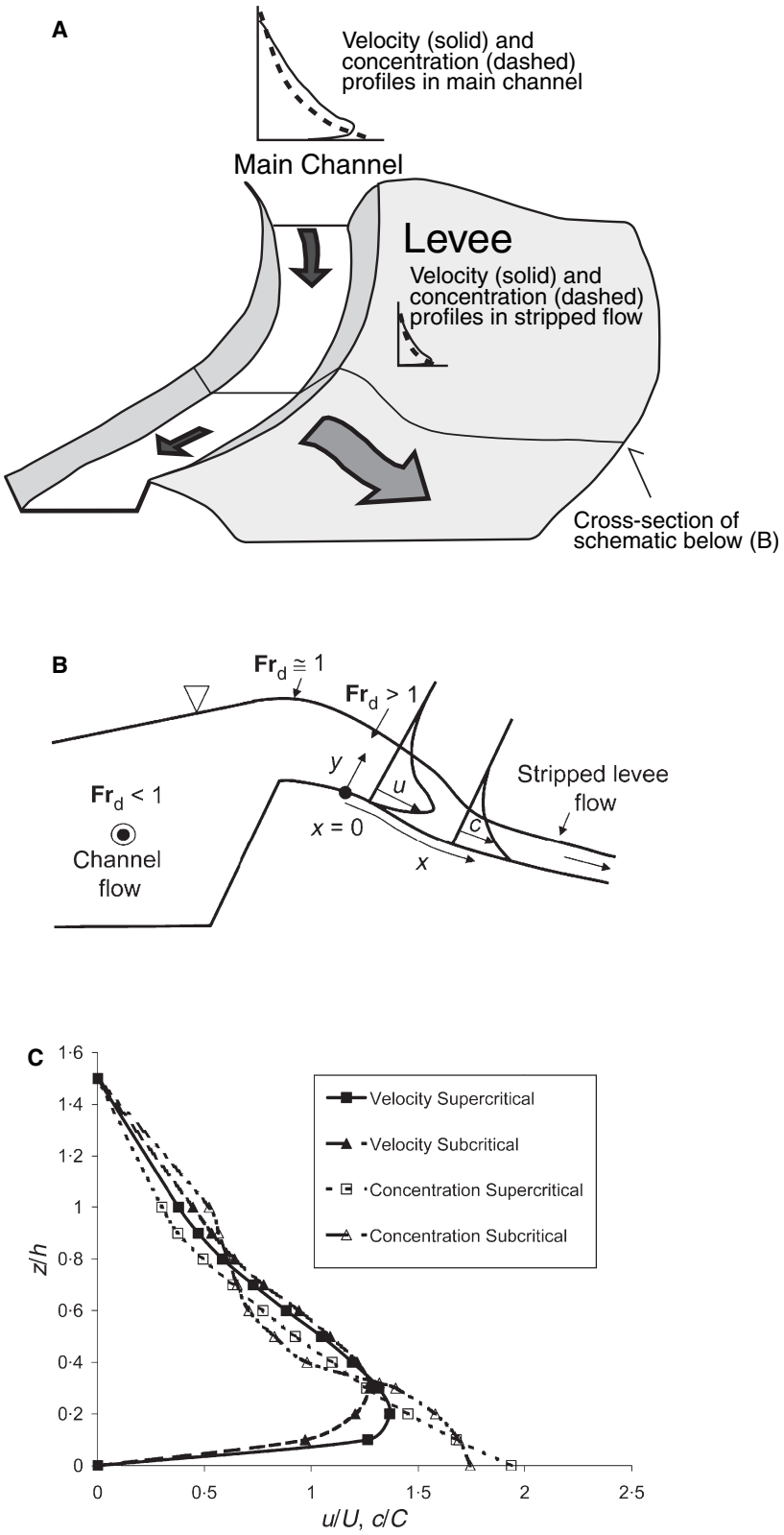

Fig. 11. (A) Illustration of the setting for the numerical model of a turbidity current created by flow stripping from the main Monterey channel over the levee on the outside of the Shepard Meander. (B) Cross section of a flow from the Monterey channel over the levee on the outside of the Shepard Meander (see text for explanation). (C) Similarity profiles for streamwise flow velocity and volume suspended-sediment concentration for sub-critical and supercritical flows, based on the saline underflows of Garcia (1993).

Calculations of the stripped turbidity current on the levee commence at a point that is some distance downstream of the levee crest (Fig. 11B). The turbidity current is approximated as a two-dimensional sheet directed down the levee and perpendicular to the direction of flow that

remained in the main channel. The boundary-attached down-levee (and thus streamwise) co-ordinate is denoted as *x*, and the boundary-attached co-ordinate upward normal to the bed is denoted as *z*. The flow in the channel is assumed to be quasi-steady, thus giving rise to a sustained, quasi-steady overspill flow onto the levee. For simplicity the sediment in the levee and the turbidity current overspilling onto it is characterized in terms of a single effective fall velocity v_s.

In the case of marine muds, the sediment may be flocculated, in which case v_s is the fall velocity of a characteristic floc. For example, Hill (1998) suggests that fine mud tends to flocculate to an effective fall velocity v_s of about 1 mm sec^{-1} in the marine setting. Assuming a specific gravity of 2·65 for the mud and the fall velocity relation of Dietrich (1982), the equivalent grain-size D of the flocs is near 33 μm.

Let $u = u(x, z, t)$, $c = c(x, z, t)$ and $k = k(x, z, t)$ and denote, respectively, the down-levee flow velocity, volume concentration of suspended sediment, and kinetic energy of the turbulence per unit mass at down-levee position *x*, upward normal position *z*, and time *t*, all averaged over turbulence. The parameters *u* and *c* can be expected to have upward-normal (essentially vertical) structures as illustrated in Fig. 11. Turbidity-current layer thickness *h*, layer-averaged down-levee flow velocity *U*, layer-averaged volume concentration *C* of suspended sediment and layer-averaged kinetic energy of the turbulence per unit mass *K* can be defined in terms of the following four moments (e.g. Ellison & Turner, 1959; Parker *et al.*, 1986):

$$Uh = \int_0^\infty u dz,\ U^2h = \int_0^\infty u^2 dz$$
$$UCh = \int_0^\infty ucdz\ UKh = \int_0^\infty ukdz \qquad (4a, b, c, d)$$

Here the limit ∞ should be interpreted to mean 'far above the turbidity current and well into the ambient water', which is assumed to be at hydrostatic equilibrium.

The four-equation model of turbidity current dynamics

The dynamics of the turbidity current are described in terms of the layer-averaged 'four-equation' model of Fukushima *et al.* (1985) and Parker *et al.* (1986). The turbidity current is assumed to be dilute in the sense that the volume concentration c satisfies the condition $c << 1$. The equation of flow mass balance of the turbidity current takes the form

$$\frac{\partial h}{\partial t} + \frac{\partial Uh}{\partial x} = e_w U \qquad (5)$$

where e_w denotes a dimensionless coefficient describing the entrainment of sediment-free ambient water from above into the turbidity current. The equation of mass conservation of sediment takes the form

$$\frac{\partial Ch}{\partial t} + \frac{\partial UCh}{\partial x} = v_s(e_s - r_o C) \qquad (6)$$

In the above equation, e_s denotes a coefficient of entrainment of bed sediment into the turbidity current per unit bed area per unit time. The vertical flux of sediment onto the bed is given as $v_s c_b$, where c_b denotes a near-bed value of suspended sediment concentration *c*. The near-bed value c_b is related to the layer-averaged value *C* by the relation

$$c_b = r_o C \qquad (7)$$

where r_o is a prescribed dimensionless parameter. Thus the term $v_s(e_s - r_o C)$ in (6) describes the net volume-rate of entrainment of sediment into suspension per unit bed area per unit time.

The equation of streamwise momentum balance is

$$\frac{\partial Uh}{\partial t} + \frac{\partial U^2 h}{\partial x} = -\frac{1}{2} Rg \frac{\partial Ch^2}{\partial x} + RgChS - u_*^2 \qquad (8)$$

In the above equation, *g* denotes the acceleration of gravity and u_* denotes the shear velocity, which is related to the bed shear stress τ_b as

$$u_* = \sqrt{\frac{\tau_b}{\rho}} \qquad (9)$$

In addition, *S* denotes streamwise (down-levee) bed slope, given as

$$S = -\frac{\partial \eta}{\partial x} \qquad (10)$$

where η denotes bed elevation. In classical treatments, the bed shear stress is related to flow

velocity in terms of a dimensionless friction coefficient c_f;

$$\tau_b = \rho u_*^2 = \rho c_f U^2 \tag{11}$$

However, the four-equation model provides a dynamic description of turbidity-current flow in terms of both the mean momentum of the streamwise flow and the mean kinetic energy per unit mass of the flow turbulence. With this in mind, Eq. (11) is replaced with the relation

$$u_*^2 = \alpha K \tag{12}$$

where α is a prescribed dimensionless parameter (see List of symbols).

The layer-averaged equation describing conservation of the kinetic energy of the turbulence takes the form

$$\frac{\partial Kh}{\partial t} + \frac{\partial UKh}{\partial x} = u_*^2 U + \frac{1}{2} U^3 e_w - \varepsilon_o h - Rgv_s Ch - \frac{1}{2} RgChUe_w - \frac{1}{2} Rghv_s(e_s - r_o C) \tag{13}$$

The first two terms on the right-hand side of Eq. (13) describe the rate of generation of turbulent kinetic energy from the mean flow. In the third term ε_o is the layer-averaged rate of dissipation of turbulent kinetic energy into heat. The fourth, fifth and sixth terms describe the interaction between the sediment and the energy balance of the flow turbulence. The fourth term is the well-known Knapp–Bagnold term (Knapp, 1938; Bagnold, 1962) describing the rate of dissipation of kinetic energy of the turbulence in holding sediment in suspension. The fifth term describes the rate of consumption of kinetic energy of the turbulence caused by the upward advection of suspended sediment in response to the entrainment of ambient water into the current (which thickens it). The final term describes the rate of consumption of kinetic energy of the turbulence as a result of the net entrainment of sediment from the bed into the flow.

The Exner equation of conservation of bed sediment (Exner, 1920, 1925) takes the form

$$(1 - \lambda_p)\frac{\partial \eta}{\partial t} = v_s(r_o C - e_s) \tag{14}$$

where λ_p denotes the porosity of the bed deposit.

Closure of Eqs (5), (6), (8), (13) and (14) require either specification of or relations for the following parameters e_w, e_s, r_o, α and ε_o. The specification of these parameters used in this paper is given in Appendix I. However, one issue does deserve elaboration.

Sediment deposits on the levees of submarine channels tend to be intricately layered, with relatively non-cohesive sandy layers interspersed with relatively cohesive muddy layers. The muddy strata tend to develop strength over time, and so resist erosion by an overriding turbidity current. There is little consensus in regard to relations for the entrainment of sub-aqueous mud into suspension (e.g. Winterwerp & Kranenburg, 2002). Available relations tend to be highly site-specific. More general relations are available for the entrainment of non-cohesive sand and coarse silt (e.g. Garcia & Parker, 1991; Wright & Parker, 2004). When these relations are applied to turbidity currents in a net erosional regime, however, they can predict spuriously high rates of bed degradation that are not consistent with the presence of even thin strata of relatively resistant material. Herein this issue is approached in a simple, empirical way. A reference entrainment rate e_{so} of bed sediment into suspension is predicted using a relation for loose, non-cohesive sediment specified in the Appendix I. The entrainment rate e_s used in Eqs (6), (13) and (14) is computed as

$$e_s = pe_{so} \tag{15}$$

where $p \leq 1$ is a limiter (Kostic & Parker 2006). In the case $p = 1$ the bed sediment is loose and easily eroded. In the case $p < 1$ the bed sediment includes layers with some strength, and so is eroded at a rate that is less than the predicted value for loose sediment.

Assumptions about the flow

The case of interest here is a Froude-supercritical flow over a levee, i.e. one satisfying the condition $\mathbf{Fr}_d > 1$, where

$$\mathbf{Fr}_d = \frac{U}{\sqrt{RgCh}} \tag{16}$$

It is not implied here that all turbidity currents over levees that result from flow stripping are necessarily supercritical flows. However, supercritical flows are necessary for the formation of upstream-migrating cyclic steps bounded by turbidity currents.

The turbidity current in the main channel from which the levee flow is stripped may be either sub-critical or supercritical. In general, steeper slopes favour supercritical flows and gentler slopes favour sub-critical flow. Because the Shepard Meander is downstream of Monterey Canyon proper, it is more likely than not that the channelized flows from which the levee flows were stripped were sub-critical. This assumption is adopted here as a convenient means of interpreting the flows. However, it is not necessary for the generation of supercritical levee flows that can generate cyclic steps.

The assumed flow configuration is summarized in Fig. 11. The levee crest constitutes a hydraulic control point, in the event that the channel flow is sub-critical, the overspilling flow should reach a densimetric Froude number of unity near the crest (Henderson, 1966; Armi & Farmer, 1985). At the levee crest, the direction of the turbidity current should be intermediate between the down-channel and down-levee directions. A short distance down levee, the stripped turbidity current should accelerate to a Froude-supercritical flow, and should also be directed essentially down-levee. The origin of the down-levee coordinate x is chosen at a point where these conditions are fulfilled.

The goal of the calculations presented here is to show the relative ease with which both depositional and erosional steps can be generated by a supercritical levee flow. The results reported are examples of a much larger set of results for which both net-erosional and net-depositional cyclic steps were observed. The initial down-levee profile consisted of a proximal reach with a length L_u of 6 km and a bed slope S_{iu} of 0·013, followed by a distal reach with a length L_d of 15 km and a bed S_{id} slope of 0·003. The numbers are loosely based on present-day down-levee profiles on the outside of the Shepard Meander. It will be seen below that the slope break at $x = 6$ km plays a role in triggering the formation of cyclic steps.

The numerical methods used in the modeling are described in Appendix II.

The upstream values U_u, h_u and C_u (flow velocity, thickness, and volume sediment concentration) at $x = 0$ are taken to be 3·5 m sec^{-1}, 20 m and 0·01, respectively. These values are derived from similarity profiles as conditioned by morphometry of the Monterey Channel and grain-size values from the core samples shown in Fig. 7. Assuming a value of R of 1·65, the upstream densimetric Froude number $\mathbf{Fr}_{du}$ is 1·95, i.e. an appropriately supercritical flow.

In the simulations, the flow over the levee is sustained for 192 hours (two cases) and 144 hours (two cases). This does not imply that a single flow of e.g. 192 hours formed the modelled bed morphologies. Rather, it implies a sequence of repeated, relatively sustained events of similar magnitude totalling 192 hours of effective flow. However, the time between events may be weeks to decades, allowing levee deposits to develop strength. This motivates the use of the limiter $p < 1$ in computing entrainment of bed sediment.

Model results: spontaneous evolution of cyclic steps

Figure 12A shows results for Case A, for which the effective grain-size was set equal to 70 μm ($v_s = 4{\cdot}05$ mm sec^{-1}) and the entrainment limiter p was set equal to 0·07. Profiles are given for both bed elevation η and interface elevation $\eta + h$. The flow begins by eroding the steep proximal initial slope. The break between proximal and distal slope triggers the formation of sediment waves. These waves are not only net-depositional, but also migrate upstream. This upstream migration eventually fills in the erosion caused earlier in the proximal zone, and also gradually regrades the average bed slope to a lesser value.

Three complete sediment waves, and the beginning of a fourth, are apparent by the end of the run. Fig. 12B shows plots of the downstream variation of the densimetric Froude number, $\mathbf{Fr}_d$, of the flow as well as the bed elevation for Case A. It is seen that each wave constitutes a step that is bounded both upstream and downstream by a hydraulic jump, where $\mathbf{Fr}_d$ changes suddenly from a value greater than unity to a value less than unity. It is based on this observation that these net-depositional sediment waves can be classified as cyclic steps.

At the end of the run, the lengths of the three steps (in order from upstream to downstream) are 6·1, 2·0 and 2·1 km. These values are of the same order of magnitude as the lengths of the first three sediment waves on the levee adjacent to the Monterey East scours. The predicted heights of the waves in Fig. 12A are in the range of $20 \sim 30$ m, decreasing downstream. The same downstream trend is apparent in the field data with wave heights in the range from 15 to 50 m.

Figure 13A shows the results for Case B1, which is identical to Case A except that effective grain-size D has been reduced to 30 μm (effective fall velocity $v_s = 0{\cdot}82$ mm sec^{-1}). The slope break

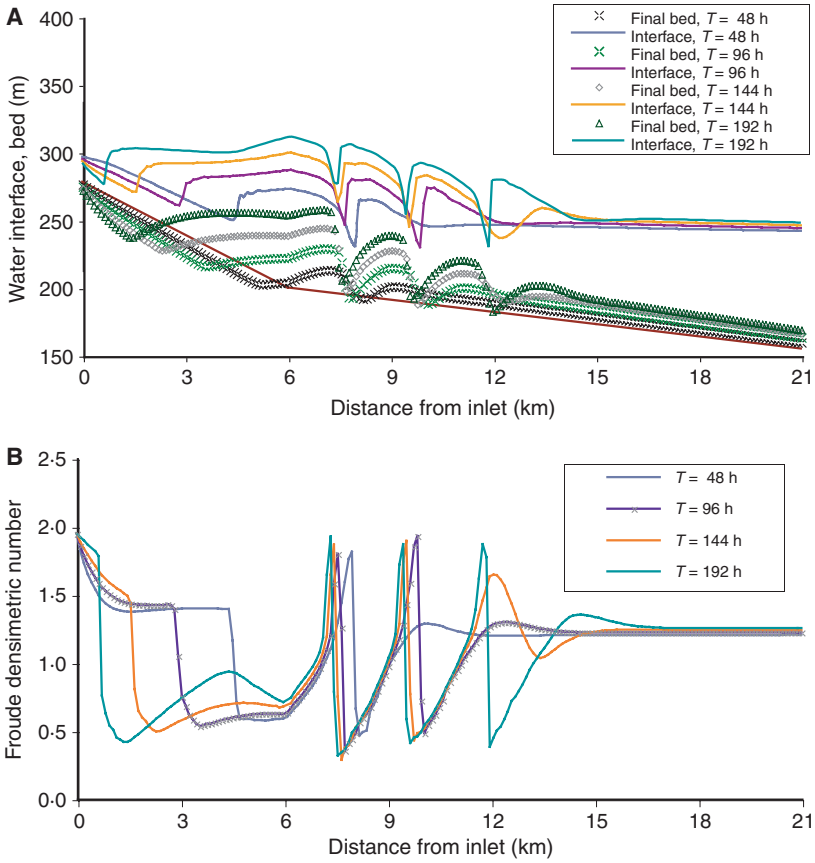

Fig. 12. (A) Results of the numerical simulation for Case A; plots show the initial bed long profile and the bed and turbidity current upper-interface long profiles at four subsequent times. (B) Results of the numerical simulation for Case A; plots of the long profiles of densimetric Froude number $\mathbf{Fr}_d$ for four times illustrating the presence of repeated hydraulic jumps.

at $x = 6$ km again triggers the formation of three steps. In this case the bed erodes everywhere except in a short reach near $x = 13$ km. Two upstream-migrating steps are clearly visible; the upstream step has a length of 9·0 km and a downstream length of 4·4 km. A third step is seen to be forming downstream. The plot of Froude number in Fig. 13B confirms that these waveforms are also cyclic steps bounded by hydraulic jumps. The step lengths are consistent with those shown in the Monterey East scours (Fig. 3). In addition, the fact that the net-erosional steps of Case B1 are longer than the net-depositional steps of Case A is also consistent with the Monterey East system (Fig. 5).

The controls on step formation are illustrated by comparing the results for Case B1 to those for Cases B2, B3 and B4, all of which pertain to the same conditions as Case B1 except for the value of the sediment entrainment limiter p, which takes the values 0·07, 0·1, 0·2 and 0·3 for cases B1, B2, B3 and B4. (In addition, Cases B3 and B4 have durations of 144 h of flow, as opposed to 192 h for Cases A, B1 and B2.)

The predicted bed and interface profiles for Cases B2, B3 and B4 are determined using the relations from Garcia (1993). An increasing value of p leads to a higher erosion rate in the steep proximal reach. The extra sediment so entrained is available for deposition downstream of the slope break. None of the cases B1 ∼ B4 are everywhere either net-erosional or net-depositional, but it is clear that lower values of p are conducive to net-erosional flows and higher values are conducive to net-depositional flows. In addition, step length decreases, and thus the number of steps that form in the modelled domain increase, as p increases. In Fig. 14C there are seven identifiable steps, justifying the terminology 'cyclic steps'.

The five cases illustrated here thus cover conditions from steps that are net-depositional everywhere to steps that are net-erosional nearly everywhere. They provide strong evidence for the following conclusions.

1 The net-depositional sediment waves on the outside levee of the Shepard Meander of the Monterey Channel are cyclic steps associated with supercritical overspill that evolves into a flow undergoing a series of hydraulic jumps. By implication, the net-depositional sediment waves

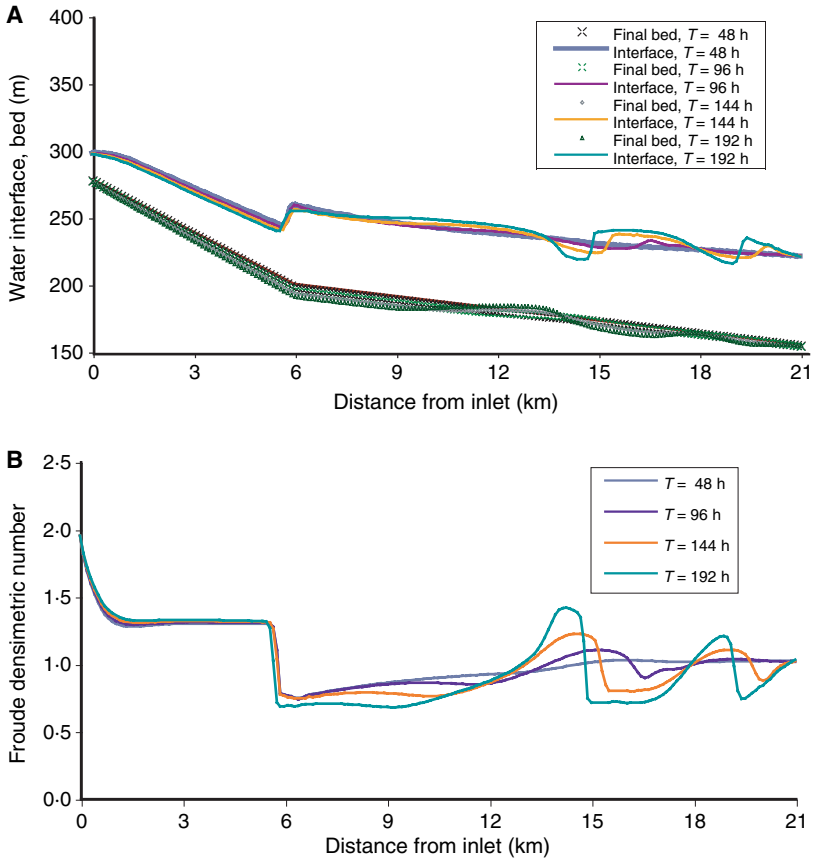

Fig. 13. (A) Results of the numerical simulation for Case B1; plots showing the initial bed long profile and the bed and turbidity current upper-interface long profiles at four subsequent times. (B) Results of the numerical simulation for Case B1; plots of the long profiles of densimetric Froude number $\mathbf{Fr}_d$ for four times illustrating the presence of repeated hydraulic jumps.

observed on the levees of many other submarine channels might also be net-depositional cyclic steps.

2 The net-erosional series of scour holes in the Monterey East system may also be cyclic steps that have been carved into the outer levee of the Monterey East channel. They are in some sense analogous to the cyclic steps produced by supercritical river flow over bedrock and cohesive material.

The precise set of events which led to the transition from net-depositional to net-erosional down-levee flow on the outside levee of the Shepard Meander are not modelled here. It is likely that the late Pleistocene erosional downcutting of 100–200 m within the Shepard Meander (Normark, 1999) is related to the change. However, Izumi (2004) has shown that net-erosional turbidity currents tend to focus. As the flow concentrates, the erosion rate is intensified, leading to the formation of a channel in the topographic low. Evidently, at some point the overspilling flows on the Shepard Meander changed from net-depositional to net-erosional, and took advantage of a slight (and perhaps random) topographic low to carve out the Monterey East scours.

Interpretation of the flows

The process of flow stripping is not modelled here. It is nevertheless of value to interpret how a levee flow with the values $U_u = 3{\cdot}5$ m sec^{-1}, $h_u = 20$ m and $C_u = 0{\cdot}01$ might be generated (as before using similarity-profile analysis). The computations given below are not meant to be precise, but rather to give a plausible picture of the main flow in the Monterey channel from which the levee flow is stripped.

Parker *et al.* (1987) and Garcia (1993) have modelled both turbidity currents and their close relatives, saline underflows in the laboratory. These flows obey at least approximate similarity profiles, e.g. u/U can be approximated as a quasi-universal function of z/h. The shape of this function differs depending on whether the flow is sub-critical or supercritical; it is also a weak function of grain-size.

Garcia (1993) has presented similarity profiles for saline underflows. Saline underflows are described by the same Eqs (5), (6), (8) and (13) as turbidity currents, in the limit as fall velocity $v_s \to 0$. Let ρ_a denote the density of the ambient fresh water above the saline underflow, and $\Delta\rho$

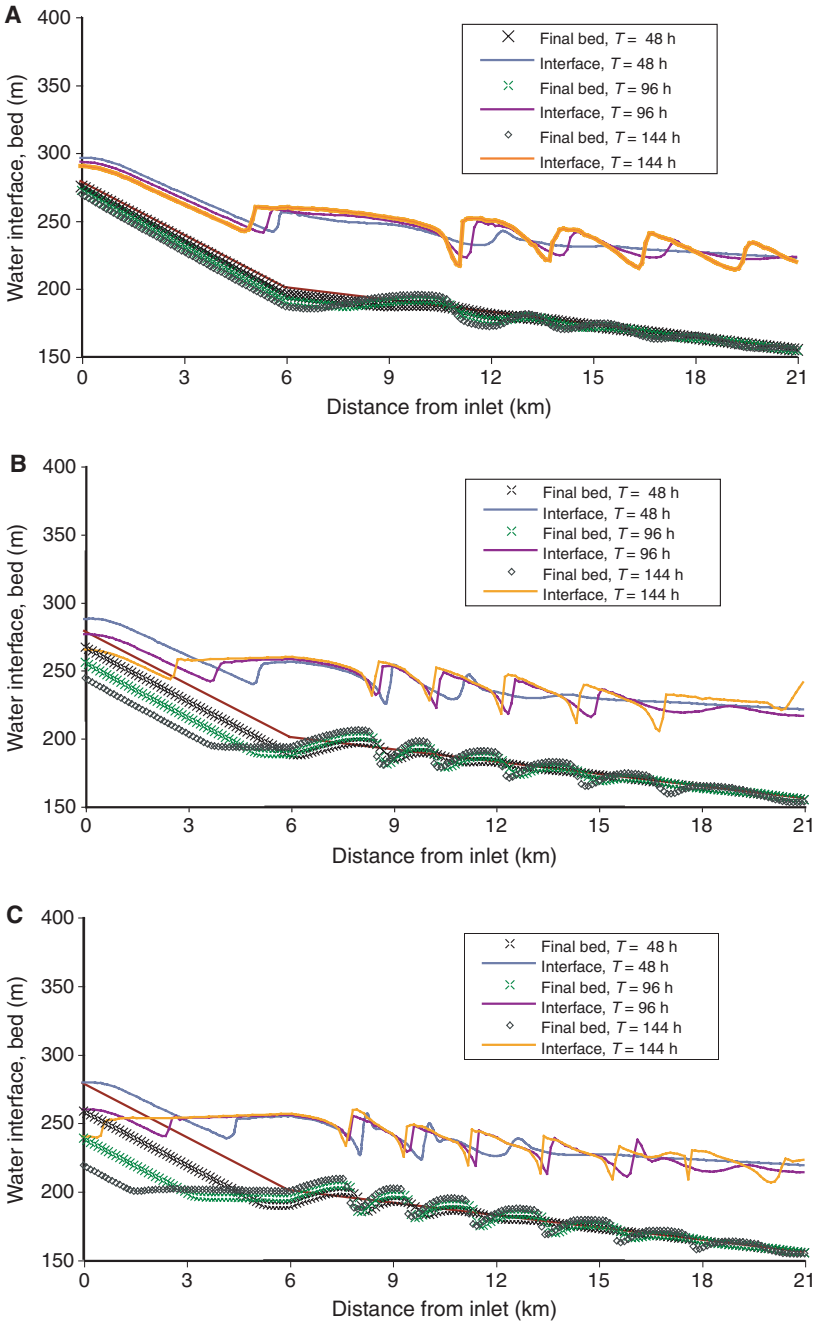

Fig. 14. (A) Results of the numerical simulation for Case B2; plots showing the initial bed long profile and the bed and turbidity current upper-interface long profiles at three subsequent times. (B) Results of the numerical simulation for Case B3; long profiles as described in A. (C) Results of the numerical simulation for Case B4 as described in A.

denote the local density difference (averaged over turbulence) at elevation z between the saline water and the fresh water above. An equivalent concentration of suspended sediment c (with infinitesimal fall velocity) can be computed in terms of an equivalent density difference, such that

$$Rc = \frac{\Delta\rho}{\rho_a} \tag{17}$$

The above relation allows the translation of the similarity profiles for saline underflows to equivalent profiles for turbidity currents. These take the form

$$\frac{u}{U} = f_{usub}\left(\frac{z}{h}\right), \quad \frac{c}{C} = f_{csub}\left(\frac{z}{h}\right) \tag{18a,b}$$

for sub-critical flow and

$$\frac{u}{U} = f_{usup}\left(\frac{z}{h}\right), \quad \frac{c}{C} = f_{csup}\left(\frac{z}{h}\right) \tag{19a,b}$$

for supercritical flow. Forms for these functions were extracted from Garcia (1993) and given in Fig. 11C.

These similarity profiles yield several parameters that are useful in interpreting the flows. Let u_{max} denote the maximum velocity of a turbidity current, and let z_{umax} denote the distance above the bed at which this is realized. For supercritical flow,

$$\frac{u_{max}}{U} = 1{\cdot}37,\ \frac{z_{umax}}{h} = 0{\cdot}20 \qquad (20a, b)$$

and for sub-critical flow

$$\frac{u_{max}}{U} = 1{\cdot}27,\ \frac{z_{umax}}{h} = 0{\cdot}32 \qquad (21a, b)$$

The thickness of a turbidity current h_{vis} from the bed to the visible interface between turbid and clear water is invariably larger than h itself. The value of h_{vis} can be estimated from the point where u and c approach zero (Fig. 11C). This value is about the same for supercritical and sub-critical flow;

$$\frac{h_{vis}}{h} = 1{\cdot}5 \qquad (22)$$

The maximum value of c is always realized at $z = 0$. For supercritical flow this is given from Fig. 11C as

$$\frac{c_{max}}{C} = 1{\cdot}97 \qquad (23)$$

For sub-critical flow the same figure yields

$$\frac{c_{max}}{C} = 1{\cdot}74 \qquad (24)$$

Finally, it is of value to have a relation for the value of c where $u = u_{max}$, i.e. c_{umax}. This parameter is needed only for supercritical flow; from Fig. 11C it takes the value

$$\frac{c_{umax}}{C} = 1{\cdot}45 \qquad (25)$$

The above relations and the values $U_u = 3{\cdot}5$ m sec^{-1}, $h_u = 20$ m and $C_u = 0{\cdot}01$ allow the estimation of the following flow parameters of the levee flow at $x = 0$. The thickness of flow to the visible interface $h_{vis} = 30$ m; the maximum velocity u_{max} is $4{\cdot}78$ m sec^{-1} realized at $z_{umax} = 4$ m above the bed; the volume concentration of suspended sediment c_{umax} at z_{umax} is $0{\cdot}0145$ and the maximum concentration of suspended sediment c_{max} is $0{\cdot}0194$.

The channel flow from which the levee flow is stripped is estimated with the aid of the following assumptions.

The depth from the bottom of the Monterey channel to the levee crest on the outside of the Shepard Meander is 150 m. Specifically, this is the distance from the bottom of the main Monterey channel to the bottom of the Monterey East channel where it joins the main channel (Fig. 3). The stripped turbidity current at $x = 0$ thus reaches its maximum velocity at 154 m above the bed of the main Monterey channel.

The layer-averaged flow velocity U in the main Monterey channel is 8 m sec^{-1}. This value yields a slightly sub-critical flow in the main Monterey channel, as outlined below.

Equations (19)–(25) can be used in conjunction with the above assumptions to yield the following estimates for the flow in the main Monterey channel: $h = 183$ m; $h_{vis} = 275$ m; $C = 0{\cdot}0245$; $u_{max} = 10{\cdot}2$ m sec^{-1}, $c_{max} = 0{\cdot}0427$; $\mathbf{Fr}_d = 0{\cdot}938$. The resulting velocity profiles in the main channel and the stripped flow at $x = 0$ are given in Fig. 15A, and the corresponding concentration profiles are given in Fig. 15B. Thus a strongly supercritical flow on the levee (or in the Monterey East scours) is stripped from a weakly sub-critical flow in the main Monterey channel.

DISCUSSION

The Monterey East depositional system provides an ideal opportunity to introduce the cyclic step concept that might shed light on the formation of turbidite channels through an evaluation of morphological data, seismic-reflection profiles (for the third dimension), sediment age and grain-size data, and mathematical models. This approach looks at deposition and erosion under supercritical flow conditions related to slope changes and flow stripping of turbidity currents. Monitoring of activity in the upper Monterey Canyon confirms that turbidity-current episodes are common all the way to the Monterey Channel (Johnson *et al.*, 2001; Xu *et al.*, 2004; Paull *et al.*, 2005). Radiometric dating from sites in the Monterey East system shows that it continues to be a location for turbidity-current activity.

The evolution of the Monterey East system and its role as a conduit bringing sediment to the fan are better understood with the application of the cyclic step model. Some seismic-reflection profiles normal to the ME trend appear to show a 'normal' channel-levee system while adjacent profiles show little evidence for a through-going channel and locally show apparent deposition represented by positive mounded areas (e.g.

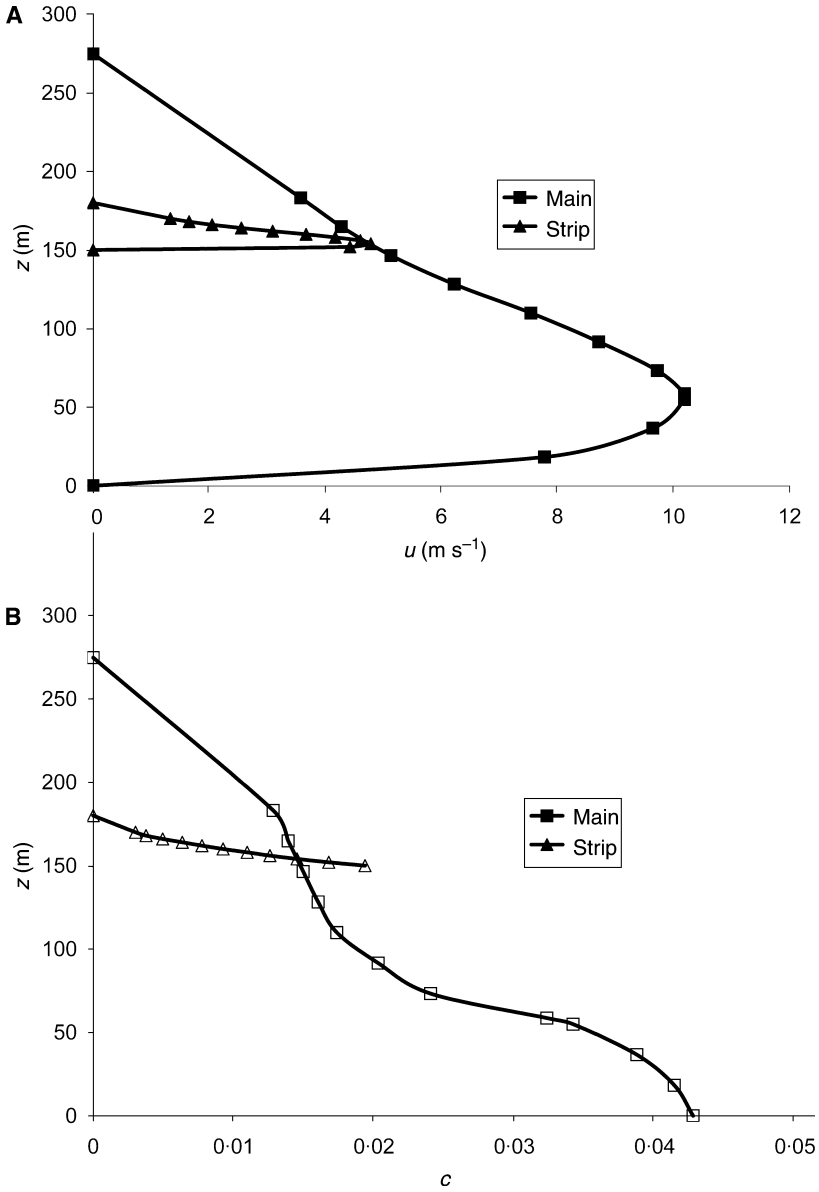

Fig. 15. (A) Interpreted streamwise flow-velocity profiles for the turbidity current in the main Monterey channel at the Shepard Meander, and the upstream region of the turbidity current stripped from flow in the main Monterey channel onto the outer levee of the Shepard Meander. (B) Interpreted streamwise volume suspended-sediment concentration profiles for the turbidity current for the same position as in A.

Fig. 4). The seismic-reflection data confirm that the scours of the ME trend are not the result of a partially filled channel. The Monterey East as interpreted could represent an early phase of channel evolution that may eventually become the main conduit extending from Monterey Canyon and result in a major avulsion.

The relationship between the line of scours and the surrounding sediment-wave field is temporal with the scours being formed last. The modeling presented here is consistent with the scour features being related to erosion and deposition by thicker turbidity currents stripped off at the site of a breech through the sediment-wave field on the levee of the Shepard Meander. More specifically, the upstream-migrating large-scale bedforms on the outside levee of the Shepard Meander appear to be net-depositional cyclic steps sculpted by turbidity currents undergoing repeated hydraulic jumps. It should be noted that once waveform topographic expression is established, the bedform can be preserved and will migrate upslope as a result of deposition from flows that are not necessarily supercritical (Wynn & Stow, 2002). The numerical analysis presented here predicts the formation of both net-depositional bedforms as well as the net-erosional cyclic steps similar to the train of scour holes observed in the Monterey East system. The net erosional steps also migrate upstream but no internal structure is preserved to demonstrate the migration as is seen for the net-depositional bedforms. A net-erosional turbidity current overflowing onto a levee can be expected to focus over time, perhaps

resulting from a breech in the levee, thus giving rise to the scours within the Monterey East system.

Radiocarbon dating of sediment from the Monterey East system shows that flow stripping of turbidity currents moving through the Monterey Shepard Meander overflow periodically throughout the Holocene (Figs 2 and 7). The presence of smaller scale bedforms (as imaged in one single pass from deep-tow sonar, Fig. 6B) suggests that volumetrically minor flows have been recently stripped at the meander bend. Overflow through the Monterey East system was probably more frequent during the latest Pleistocene, when the turbidity currents were larger and probably more common. This is shown from cores on the Monterey Ascension levee downstream from the Shepard Meander (Normark, 1999). Continued development of the Monterey East system could potentially result in avulsion with loss of sediment for Monterey channel downstream of the meander. Even during the Holocene, the larger flows that move across the Monterey East system probably rejoin the main body of the turbidity-current flow that stayed in the Monterey and Monterey-Ascension channels (Fig. 1).

CONCLUSIONS

The Monterey East depositional system lies south of the prominent Shepard Meander and has formed as a result of the flowstripping of turbidity currents moving through the meander. The system is characterized by large-scale sediment waves dissected by a linear train of giant scours incised into the levee on the outside of the Shepard Meander. Seismic-reflection data indicate a consistent upstream (updip) direction of migration for the sediment waves. Such upstream-migrating sediment waves are a ubiquitous feature of the submarine environment, being especially prominent on channel levees and near slope breaks. The analysis presented here suggests that these sediment waves are net-depositional cyclic steps rather than antidunes. Cyclic steps are related to antidunes, but in the former case the steps are locked into an upstream-migrating train by a series of hydraulic jumps, as the flow alternates from Froude-sub-critical on the upstream side of a step to Froude-supercritical on the downstream side.

Upstream-migrating cyclic steps can be net-erosional. The series of scours in the Monterey East system were formed by net-erosional turbidity currents. The net-erosional flows were probably focused through a breech in the levee, perhaps formed as a result of slumping of the steep wall within the meander as it was erosionally deepened. The Monterey East system may represent the early stage of an eventual avulsion from the present-day Monterey Channel. Linear scour-shaped depressions have been observed elsewhere, and the models developed for the Monterey East example might have broad applicability to channel formation on submarine fans.

ACKNOWLEDGEMENTS

A. F. thanks Chevron for time to pursue this project. M. McGann kindly allowed us access to unpublished radiocarbon age data for several of the core samples. D. Mosier, C. E. Gutmacher, F. L. Wong, C. H. Degnan, J. A. Reid, and M. Hamer provided valuable assistance in retrieving archived data and preparing digital images for some of the figures used in this manuscript. The manuscript was improved by reviews from Julian Thorne, Jingping Xu, Helen Gibbons, Ben Kneller, Russell Wynn, and Editor Peter Haughton. Part of the research reported in this manuscript was performed under the auspices of the National Center for Earth-surface Dynamics (NCED), a Center funded by the National Science Foundation STC Program under agreement number EAR-0120914. This research specifically addresses the NCED research effort on channels.

LIST OF SYMBOLS

a	constant in the sediment entrainment relation
c_b	near-bed concentration of suspended sediment
c_f	dimensionless friction coefficient
c_f*	equilibrium value of dimensionless friction coefficient c_f
C	turbidity current depth-averaged volumetric concentration
c_{umax}	volumetric concentration of suspended sediment at z_{umax}
D	characteristic grain-size of the sediment
e_s	sediment entrainment rate
e_{so}	entrainment rate for purely non-cohesive sediment
e_w	water entrainment coefficient
f_{usub}	f_{usup} velocity similarity profile for a sub/supercritical saline underflow

f_{csub} f_{csup} concentration similarity profile for a sub/supercritical saline underflow
$\mathbf{Fr}_d$ densimetric Froude number
$\mathbf{Fr}_{du}$ upstream densimetric Froude number
g acceleration of gravity
h turbidity current thickness
h_{vis} current thickness from the bed to the clear current-ambient interface
h_0, U_0, C_0, K_0 values of h, U, C and K at the inflow boundary
K turbidity current depth-averaged turbulent kinetic energy per unit mass length of the domain
p sediment entrainment limiter
R submerged specific gravity of sediment
Ri bulk Richardson number
Re_p particle Reynolds number
r_o multiplicative constant
S_i initial bed slope
S_{iu} slope of a proximal zone
S_{id} slope of a distal zone
S_f friction slope
t time
u_* shear velocity
U turbidity current depth-averaged velocity
u_{max} max velocity of a turbidity current
v_s sediment fall velocity bottom-attached streamwise co-ordinate
z upward normal co-ordinate
z_{umax} distance above the bed associated with max velocity U_{max}
α coefficient in the closure relation for viscous dissipation rate
β coefficient in the closure relation for viscous dissipation rate
ε_o dissipation of turbulent kinetic energy
η bed elevation
η_o antecedent bed elevation
λ_p porosity of the bed deposit
γ kinematic viscosity of the water
ρ_a density of the ambient water
Δ_ρ density difference
τ_b bed shear stress
$\dot{\omega}$ velocity of the current head.

REFERENCES

Armi, L. and **Farmer, D.M.** (1985) The internal hydraulics of the Strait of Gibraltar and associated sills and narrows. *Oceanol. Acta*, **8,** 37–46.

Bagnold, R.A. (1962) Auto-suspension of transported sediment, turbidity currents. *Proc. Roy. Soc. London*, **A265,** 315–319.

Brooks, P.C. (2001) *Experimental study of erosional cyclic steps*, M.S. Thesis. University of Minnesota, London.

Dietrich, E.W. (1982) Settling velocities of natural particles. *Water. Resour. Res.*, **18,** 1626–1682.

Dill, R.F., Dietz, R.S. and **Stewart, H.B. Jr.** (1954) Deep-sea channels and delta of the Monterey submarine canyon. *Geol. Soc. Amer. Bull.*, **65,** 191–194.

Elliott, T. (2002) Megaflute erosion surfaces and the initiation of turbidite channels. *Geology*, **28,** 119–122.

Ellison, T.H. and **Turner, J.S.** (1959) Turbulent entrainment in stratified flows. *J. Fluid Mech.*, **6,** 423–448.

Engelund, F. (1970) Instability of erodible beds. *J. Fluid Mech.*, **42,** 225–244.

Engelund, F. and **Fredsoe, J.** (1982) Sediment ripples and dunes. *Annu. Rev. Fluid Mech.*, **14,** 13–37.

Exner, F.M. (1920) Zur Physik der Dunen. *Sitzber. Akad. Wiss Wien, Part IIa, Bd.* **129,** 929–952.

Exner, F.M. (1925) Uber die Wechselwirkung zwischen Wasser und Geschiebe in Flussen, Sitzber. *Akad. Wiss Wien, Part IIa, Bd.* **134,** 165–204.

Fildani, A. and **Normark, W.R.** (2004) Late Quaternary evolution of channel and lobe complexes of Monterey Fan. *Mar. Geol.*, **206,** 199–223.

Fukushima, Y, Parker, G. and **Pantin, H.M.** (1985) Prediction of ignitive turbidity currents in Scripps Submarine Canyon. *Mar. Geol.*, **67,** 55–81.

Garcia, M. (1993) Hydraulic jumps in sediment-driven bottom currents. *J. Hydraul. Eng.*, **119,** 1–24.

Garcia, M.H. and **Parker, G.** (1991) Entrainment of bed sediment into suspension. *J. Hydraul. Eng.*, **117,** 414–435.

Henderson, F.M. (1966) *Open Channel Flow*. Macmillan, New York, 522 p.

Hess, G.R. and **Normark, W.R.** (1976) Holocene sedimentation history of the major fan valleys of Monterey Fan. *Mar. Geol.*, **22,** 233–251.

Hill, P.S. (1998) Controls on floc size in the coastal ocean. *Oceanography*, **11,** 13–18.

Izumi, N. (2004) The formation of submarine gullies by turbidity currents. *J. Geophys. Res.*, **109,** C03048, doi:10·1029/2003JC001898 13 p.

Johnson, K.S., Paull, C.K., Barry, J.P. and **Chavez, F.P.** (2001) A decadal record of underflows from a coastal river into the deep sea. *Geology*, **29,** 1019–1022.

Knapp, R.T. (1938) Energy balance in streams carrying suspended load. *Trans. Am. Geophys. Union*, **1,** 501–505.

Kostic, S. and **Parker, G.** (2003) Progradational sand-mud deltas in lakes and reservoirs: Part 1. Theory and numerical modeling. *J. Hydraul. Res.*, **41,** 127–140.

Kostic, S. and **Parker, G.** (2006) The response of turbidity currents to a canyon-fan transition: internal hydraulic jumps and depositional signatures. *J. Hydraul. Res.* (in press).

Koyama, T. and **Ikeda, H.** (1998) Effect of riverbed gradient on bedrock channel configuration: a flume experiment. *Proc. Environ. Res. Center, Tsukuba University, Japan*, **23,** 25–34.

Launder, B.E. and **Spalding, D.B.** (1972) *Lectures in Mathematical Models of Turbulence*. Academic Press, London.

Lee, H.J., Syvitski, J.P.M., Parker, G., Orange, D., Locat, J., Hutton, E.W.H. and **Imran, J.** (2002) Distinguishing sediment waves from slope failure deposits: field examples, including the 'Humboldt slide' and modelling results. *Mar. Geol.*, **192,** 79–104.

Leonard, B.P. (1979) A stable and accurate convection modeling procedure based on quadratic upstream interpolation. *Comp. Methods Appl. Mech. Eng.*, **19,** 59–98.

Leonard, B.P. (1991) The ULTIMATE conservative difference scheme applied to unsteady one-dimensional advection. *Comp. Methods Appl. Mech. Eng.*, **88,** 17–77.
Lien, T., Walker, R.G. and **Martinsen, O.J.** (2003) Turbidites in the Upper Carboniferous Ross Formation, western Ireland: reconstruction of a channel and spillover system. *Sedimentology*, **50,** 113–148.
McHugh, C.M.G. and **Ryan, W.B.F.** (2000) Sedimentary features associated with channel overbank flow: examples from the Monterey Fan. *Mar. Geol.*, **163,** 199–215.
McHugh, C.M.G., Ryan W.B.F. and **Hecker, B.** (1992) Contemporary sedimentary processes in the Monterey Canyon-fan system. *Mar. Geol.*, **107,** 35–50
Menard, H.W. (1955) Deep-sea channels, topography, and sedimentation. *AAPG Bull.*, **39,** 236–255.
Mutti E. and **Normark, W.R.** (1987), Comparing examples of modern and ancient turbidite systems: problems and concepts. In: *Marine Clastic Sedimentology: Concepts and Case Studies* (Eds J. K. Leggett and G. G. Zuffa), p. 1–38. Graham and Trotman, London.
Normark, W.R. (1970a) Channel piracy on Monterey deep-sea fan. *Deep-Sea Res.*, **17,** 837–846.
Normark, W.R. (1970b) Growth patterns of deep-sea fans. *AAPG Bull.*, **54,** 2170–2195.
Normark, W.R. (1999) Late Pleistocene channel-levee development on Monterey submarine fan, central California. *Geo-Mar. Lett.*, **18,** 179–188.
Normark, W.R. and **Gutmacher, C.E.** (1988) Sur submarine slide, Monterey Fan, central California. *Sedimentology*, **35,** 629–647.
Normark, W.R., Piper, D.J.W. and **Hess, G. R.** (1979) Distributary channels, sand lobes, and mesotopography of navy submarine fan, California Borderland, with applications to ancient fan sediments. *Sedimentology*, **26,** 749–774.
Normark, W.R., Gutmacher, C.E., Chase, T.E. and **Wilde, P.** (1985) Monterey Fan, Pacific Ocean. In: *Submarine Fans and Related Turbidite Systems* (Eds A.H., Bouma, W.R., Normark, N.E., Barnes), pp. 79–86. Springer-Verlag, New York.
Normark, W.R., Piper, D.J.W., Posamentier, H., Pirmez, C. and **Migeon, S.** (2002) Variability in form and growth of sediment waves on turbidite channel levees. *Mar. Geol.*, **192,** 23–58.
Parker, G. and **Izumi, N.** (2000) Purely erosional cyclic and solitary steps created by flow over a cohesive bed. *J. Fluid Mech.*, **419,** 203–238.
Parker, G., Fukushima, Y. and **Pantin, H.M.** (1986) Self-accelerating turbidity currents. *J. Fluid Mech.*, **171,** 145–181.
Parker, G., Garcia, M., Fukushima, Y. and **Yu, W.** (1987) Experiments on turbidity currents over an erodible bed. *J. Hydraul. Res.*, **25,** 123–147.
Paull, C.K., Mitts, P., Ussler, W. III, Keaten, R. and **Greene, H.G.** (2005) Trail of sand in Upper Monterey Canyon, Geol. *Soc. Am. Bull.*, **117,** 1134–1145.
Piper, D.J.W. and **Normark, W.R.** (1983) Turbidite depositional patterns and flow characteristics, Navy submarine fan, California Borderland. *Sedimentology*, **30,** 681–694.
Pirmez, C. and **Imran, J.** (2003) Reconstruction of turbidity currents in Amazon Channel. *Mar. Petrol. Geol.*, **20,** 823–849.
Prothero, D.R. and **Schwab, F.** (1996) *Sedimentary Geology*. W. H. Freeman and Co., New York, 575 p.
Reid, L.M. (1989) Channel incision by surface runoff in grassland catchments. PhD. Thesis. University of Washington, Washington.
Shepard, F.P. (1966) Meander in valley crossing a deep-sea fan. *Science*, **154,** 385–386.
Sun, T. and **Parker, G.** (2005) Transportational cyclic steps created by flow over an erodible bed. Part 2. Theory and numerical simulation. *J. Hydraul. Res.* **43,** 502–514.
Taki, K. and **Parker, G.** (2005) Transportational cyclic steps created by flow over an erodible bed. Part 1. Experiments. *J. Hydraul. Res.* **43,** 488–501.
Winterwerp, J.C. and **Kranenburg, C.** (2002) *Fine Sediment Dynamics in the Marine Environment. Proceedings in Marine Science 5*. Elsevier Science, Amsterdam, 713 pp.
Winterwerp, J.C., Bakker, W.T., Mastbergen, D.R. and **van Rossum, H.** (1992) Hyperconcentrated sand-water mixture flows over erodible bed. *J. Hydraul. Eng.*, **119,** 1508–1525.
Wohl, E.E. (2000) Substrate Influences on Step-Pool Sequences in the Christopher Creek Drainage, Arizona. *Geology*, **108,** 121–129.
Wright, S. and **Parker, G.** (2004) Flow resistance and suspended load in sand-bed rivers: simplified stratification model. *J. Hydraul. Eng.*, **130,** 796–805.
Wynn, R.B. and **Stow, D.A.V.** (2002) Classification and characterisation of deep-water sediment waves. *Mar. Geol.*, **192,** 7–22.
Xu, J.P., Noble, M.A. and **Rosenfeld, L.K.** (2004) In-situ measurements of velocity structure within turbidity currents, Geophys. *Res. Lett.*, **31,** L09311, doi:10·1029/2004GL019718.

Manuscript received 14 May 2005; revision accepted 7 June 2006

APPENDIX I: CLOSURE RELATIONS AND PARAMETERS OF THE FOUR-EQUATION MODEL

Internal relations and parameters employed to close the governing Eqs (5), (6), (8), (13) and (14) of the model are listed below. The coefficient of water entrainment is specified in accordance to the relation of Fukushima *et al.* (1985) for density underflows:

$$e_{\mathrm{w}} = \frac{0{\cdot}00153}{0{\cdot}0204 + \mathbf{Ri}} \qquad (A1)$$

In the above relation **Ri** denotes the bulk Richardson number, given by

$$\mathbf{Ri} = \frac{RghC}{U^2} \qquad (A2)$$

The densimetric Froude number $\mathbf{Fr}_{\mathrm{d}}$ is defined in Eq. (2); it is related to the Richardson number as

$$\mathbf{Ri} = \mathbf{Fr}_{\mathrm{d}}^{-2} \qquad (A3)$$

The coefficient of entrainment of bed sediment e_{s} by submarine turbidity currents is related to a reference entrainment rate for purely non-cohesive sediment e_{so}, using an erosion limiter $p \leq 1$,

such that the computed entrainment rate e_s becomes equal to pe_{so} (15). The reference rate e_{so} is calculated using the following formulation by Wright & Parker (2004) for the full range of field-scale rivers:

$$e_{so} = \frac{aZ^5}{1 + \frac{a}{0{\cdot}3}Z^5} \qquad (A4)$$

where a is a constant equal to $7{\cdot}8 \times 10^{-7}$, and

$$Z = \frac{u_*}{v_S}\mathbf{Re}_p^{0{\cdot}6}S_f^{0{\cdot}08} \qquad (A5)$$

In the above relation, $\mathbf{Re}_p$ denotes a particle Reynolds number and S_f denotes a friction slope, evaluated as follows:

$$\mathbf{Re}_p = \sqrt{RgD}D/v \qquad (A6)$$

$$S_f = \frac{u_*}{gh} \qquad (A7)$$

In the above relations, D denotes the characteristic grain-size of the sediment and v denotes the kinematic viscosity of water.

Equation (13) of the conservation of turbulent kinetic energy requires one more closure relation for the viscous dissipation rate ε_o. In general, this parameter may be specified in the following manner (e.g. Launder & Spalding, 1972):

$$\varepsilon_o = \beta\frac{K^{1{\cdot}5}}{h} \qquad (A8)$$

where according to Fukushima *et al.* (1985) and Parker *et al.* (1986)

$$\beta = \left[\frac{1}{2}e_w\left(1 - Ri - 2\frac{c_f^*}{\alpha}\right) + c_f^*\right] \Big/ \left(\frac{c_f^*}{\alpha}\right)^{1{\cdot}5} \qquad (A9)$$

In the above relation c_f* is an 'equilibrium' coefficient of bed friction as defined by Fukushima *et al.* (1985).

In all simulations presented herein, the prescribed constants r_o and are set equal to 2 and 0·1, respectively.

APPENDIX II: NUMERICAL ALGORITHM

A turbidity current forms a distinct head, or front as it evolves. Here, the dynamics of the turbidity current are solved on a grid that deforms in space and time. The outflow boundary is located at, and moves with, the front until such time as it migrates beyond a domain of interest of specified length L. After that time the outflow boundary is simply the downstream end of the specified domain. Initial and boundary conditions for the numerical model are discussed in more detail in Kostic & Parker (2006). An initial front position is specified, and the initial values of the dependent variables h, U, C and K at all nodal points up to the initial position of the front are set equal to their values h_o, U_o, C_o and K_o at the inflow boundary located at $x = 0$. The initial bed elevation for every grid point is specified in terms of a proximal zone with a length of 6 km and a slope S_{Iu} of 0·013, and a distal zone with a length of 15 km and a slope S_{Id} of 0·003, so that the length L of the domain is 21 km. The numerical model, however, can encompass an arbitrary initial bed profile. Supercritical flow is specified at the inflow boundary, where three physical boundary conditions are prescribed as follows:

$$h(x = 0, t) = h_o, U(x = 0, t) = U_o, C(x = 0, t) = C_o \qquad (A10)$$

At the outflow boundary two physical conditions are required as long as the turbidity current has not propagated out of the domain, which here has a length of 21 km. These conditions are formulated as follows:

$$U(x = L, t) = \dot{\omega},\ \eta(x = L, t) = \eta_0(L) \qquad (A11)$$

where $\dot{\omega}$ denotes the front velocity, and η_o is the antecedent bed elevation as yet unmodified by the turbidity current (because the current has not yet reached the bed there). Once the current covers the entire length of the domain no physical condition is imposed at the outflow boundary.

The governing equations together with the previously discussed initial and boundary conditions, are solved numerically by means of the ULTIMATE QUICKEST scheme (Leonard, 1979, 1991). This explicit finite-volume upwind algorithm is particularly suitable for highly advective unsteady flow problems. A more comprehensive interpretation of the numerical model can be found in Kostic & Parker (2003, 2006).

